2nd URSI AT-RASC, Gran Canaria, 28 May – 1 June 2018

Numerical Study of Statistical Properties of Stored and Dissipated Energy in Reverberant Cavities

Mihai I. Andries[(1)], Luk R. Arnaut*[(2)]
(1) DB Technology, Cambridge CB23 8PS, United Kingdom
(2) Queen Mary University, London E1 4FZ, United Kingdom

Abstract

Based on full-wave numerical simulation data, the spatial probability distributions of stored and dissipated energies inside a static lossy overmoded cavity are characterized. The spectral fluctuations and variation of the quality factor show a significant dependence on the wall conductivity.

1. Introduction

Overmoded cavities (often referred to as reverberation chambers) provide a paradigm for emulating real-world complex electromagnetic propagation environments. Although the frequency dependence of their averaged field properties is different from that in free-space multipath propagation, such cavities nevertheless provide useful physical insight and representation of quasi-random electromagnetic fields. This can be done for mechanically static as well as for dynamic scenarios, for example for applications to wireless mobile communications. In this work, only static configurations are considered.

Inside a reverberation chamber of interior volume V and surface area S, the transmission loss between the transmitted power P_T and the volume averaged received power $\langle P_R \rangle_V$ is governed by the quality factor Q via

$$\langle P_R \rangle_V = \frac{\lambda^3 Q}{16\,\pi^2 V} P_T, \qquad (1)$$

where $Q = \omega U / P_d$ characterizes to the ratio of the time-averaged stored energy U inside V to the energy loss per cycle (i.e., dissipated power P_d) across S. However, in order to compare differences between free-space and cavity transmission loss, it is of interest to study the energy storage and energy loss individually. Since multipath and overmoded environments exhibit complex spatial variation of their field, it is useful to investigate the feasibility of employing a statistical framework to characterize the spatial fluctuations based on their probability distribution [1], even for integrable (non-chaotic) cavities.

The practical evaluation of Q is often limited to estimates based on *local* measurements, e.g., those based on S-parameters at the location of the antennas, r [2]. In order to evaluate the spatially aggregated energies as required in the definition of Q, it is therefore of interest to apply full-wave numerical simulation. In this paper, we present results based on finite integration time domain (FITD) field simulations inside a lossy parallelepiped overmoded cavity excited by a quarter-wavelength monopole antenna. Boundary and interior field data are analyzed separately to obtain the empirical probability distributions of their respective associated energies. These are then compared with theoretical distributions.

2. Numerical Simulations

FITD simulations (using CST Microwave Studio®) were performed across the frequency range 950-1049.9 MHz using a frequency step of 150 kHz. Because of limited time and computational resources, the Cartesian components of the E- and H-fields across the entire cavity volume and boundary were evaluated only at 61 frequencies across the band 995.425-1004.425 MHz.

The simulated model is a simple parallelepiped cavity of dimensions 8.7×3.7×2.9 m^3, as depicted in Figure 1. The boundaries of the simulation cavity are nonmagnetic metal walls with a conductivity of σ_w = 10,000 S/m. No other losses are considered. A quarter-wavelength monopole antenna of nondimensional radius is used for the cavity excitation. It is placed 4 mm above the cavity floor (8.7×3.7 m^2) and 1.2 m from the nearest vertical walls. The length of the monopole is adapted for the simulation range. The interior volume and the antenna are spatially discretized using adaptive hexahedral meshing. The smallest and largest spacing between any two adjacent grid points are 4 mm and 28.5 mm, respectively. This results in 4,264,818 mesh cells.

The excitation port is located between one end of the monopole, at 4 mm above the floor surface, and its projection onto the floor. The excitation signal is a 100 MHz-wide Gaussian pulse, adapted for the range 950-1049.9 MHz. Within the bandwidth of the virtual receiver (995.425-1004.425 MHz), the frequency response of this pulse has a variation of less than 0.16 dB.

The convergence criterion for terminating the time-domain simulation is the crossing of a threshold at -50 dBc for the decaying normalized power, evaluated at the excitation port and shown in Figure 2, or for reaching a maximum simulation time of 50 μs, whichever condition is met first.

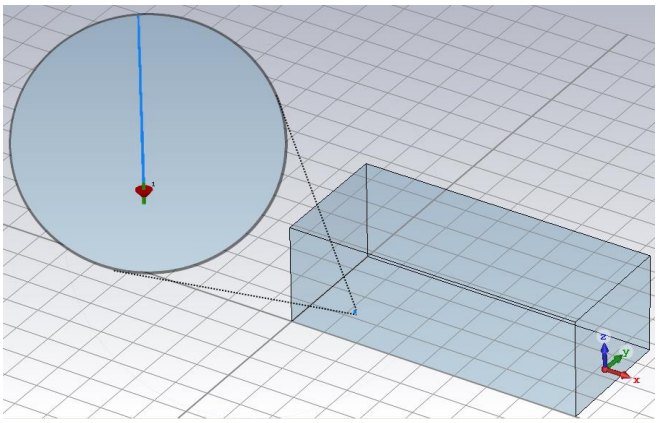

(a)

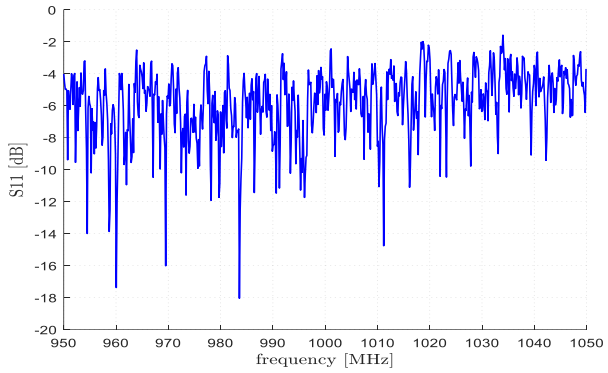

(b)

Figure 1: (a) Simulated resonant cavity and excitation monopole. (b) In-situ $|S_{11}(f)|$ of the monopole antenna.

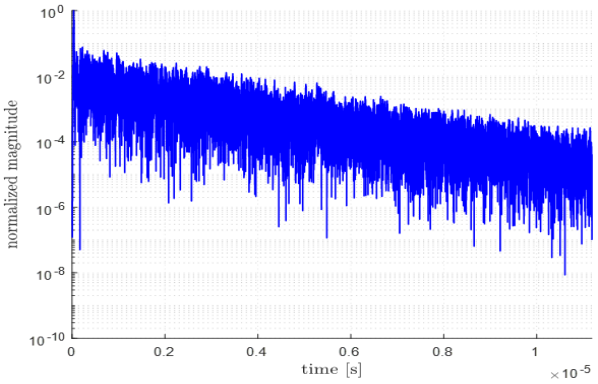

Figure 2: Time-domain amplitude response of the chamber evaluated at the location of the monopole antenna.

3. Numerical Results

Simulations for the real and imaginary parts of the Cartesian E- and H-field components were performed consecutively, at the same grid points. The data along the X-, Y- and Z-axes were exported for step sizes of 150 mm, 148 mm, and 145 mm, respectively, in order to obtain an integer number of locations along each axis. This corresponds to $59 \times 26 \times 21 = 32{,}214$ locations for the field evaluation, of which 6,222 are located on the boundaries.

As an example, the amplitudes of the total (vector) E- and H-fields in the (X,Y)-plane at the height z = 1.45 m and frequency f = 1000.08 MHz are shown in Figure 3. The corresponding spatial orientations of the field vectors in this plane for zero phase are shown in Figure 4.

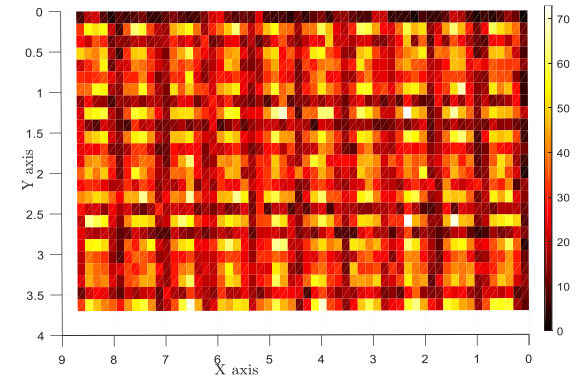

(a)

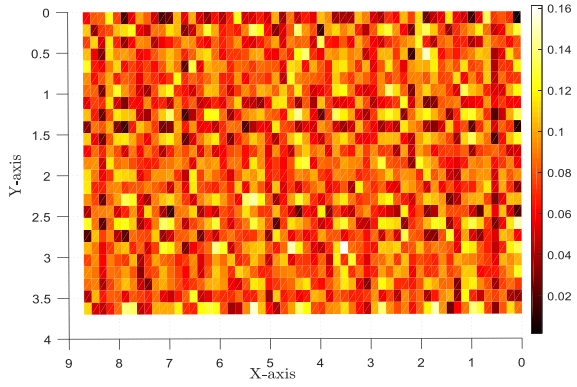

(b)

Figure 3: Amplitudes of simulated (a) E-field (V/m) and (b) H-field (A/m) at z = 1.45 m and f = 1000.08 MHz.

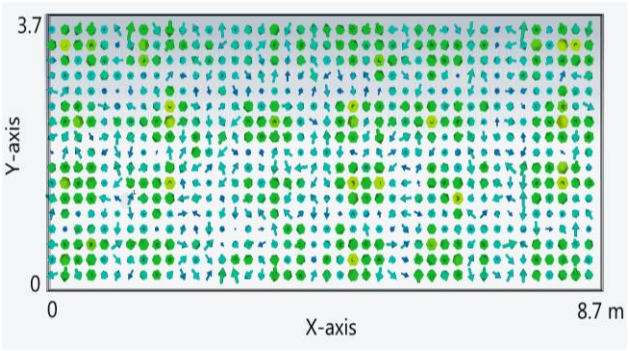

(a)

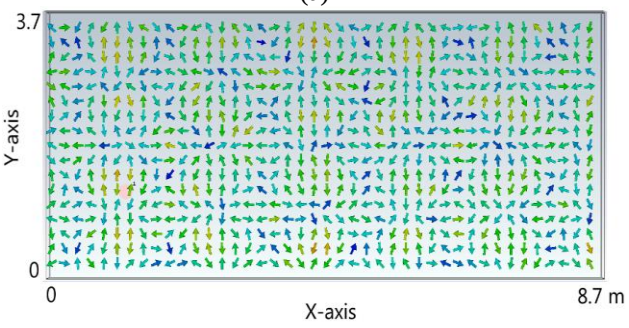

(b)

Figure 4: Spatial orientation of the (a) E- and (b) H-field vectors for zero phase, corresponding to Figure 3.

Conversely, Figure 5 shows the frequency response of the E- and H-field amplitudes at (x=4.35, y=1.776, z=1.45) m.

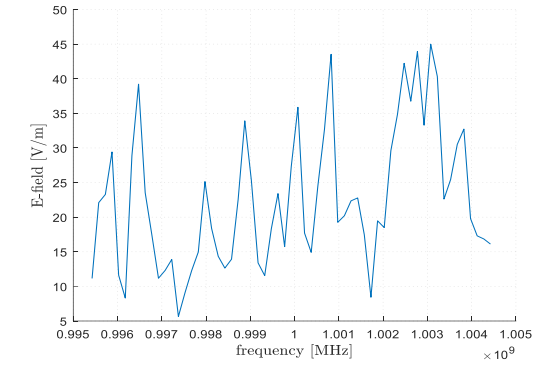

(a)

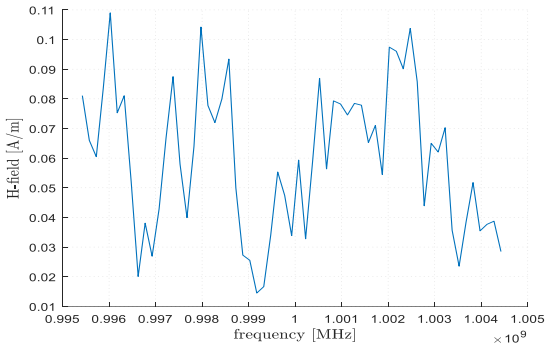

(b)

Figure 5: Field variation across simulated frequency range at (x=4.35, y=1.776, z=1.45) m: (a) E-field and (b) H-field.

4. Statistical Analysis

From the magnetic field data, Q can be estimated from the interior field H and the tangential boundary field H_t as [1]

$$Q = \frac{2}{\delta_w} \frac{\iiint_V \left|\underline{H}(\underline{r})\right|^2 \mathrm{d}V}{\iint_S \left|\underline{H}_t(\underline{r}_S)\right|^2 \mathrm{d}S}, \qquad (2)$$

where δ_w is the skin depth of the walls. Figure 6a shows $Q(f)$ at σ_w = 10,000 S/m and Figure 6b shows the mean-normalized standard deviation σ_Q/μ_Q across the 61 simulated frequencies for selected values of σ_w. The results demonstrate that $Q(f)$ exhibits rapid spectral fluctuations and that the magnitude of the fluctuations of $Q(f)$ rapidly increases with decreasing wall losses.

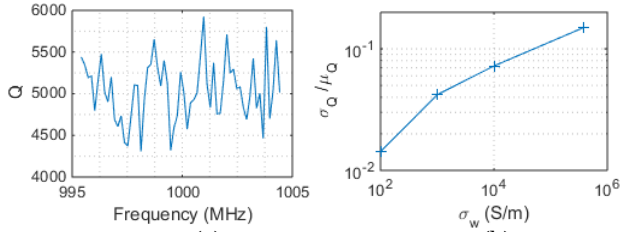

(a) (b)

Figure 6: (a) $Q(f)$ for σ_w = 10,000 S/m. (b) Coefficient of spectral variation of Q as a function of conductivity σ_w.

Figure 7 presents the local magnetic energies, viz., the stored $|\underline{H}(\underline{r})|^2$ and dissipated energy $|\underline{H}_t(\underline{r}_S)|^2$ at f = 995.575 MHz as a function of linear scan locations $\underline{r}$ and $\underline{r}_S$, respectively. The scanning process is unidirectional and parallel to the X-axis, in planes parallel to the (X,Y)-plane, from (0, 0, 0) to (58, 25, 20). The boundary field scans are shown in the order (z=0, z=2.9, y=0, y=3.7, x=0, x=8.7) m.

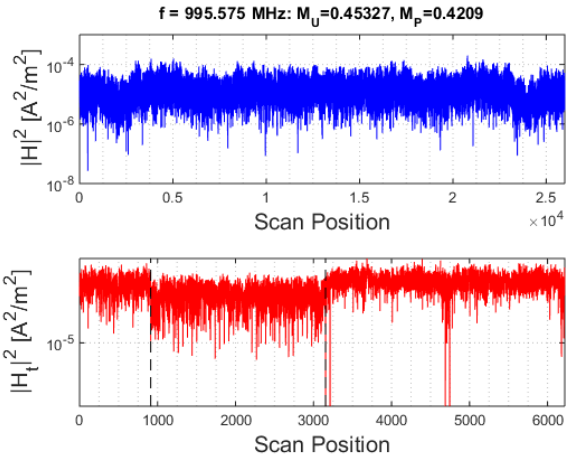

Figure 7: Stored interior energy (top) and dissipated boundary energy (bottom) position at f = 995.575 MHz as a function of scan position.

The analysis at this and other frequencies within the simulated band indicates that the dissipated energy shows statistical heterogeneity between the three pairs of parallel boundaries, at break points separated by 912, 2242 and 3068 scan points, respectively. This heterogeneity is attributable to the asymmetric location of the antenna (relative to the wavelength) with respect to these boundaries. It has been verified that this heterogeneity can be eliminated by source stirring of the antenna, or by renormalizing with respect to the dissipated energy per pair of parallel planes.

Figure 8 shows theoretical (dashed) $\chi^2_{6M_U}$ and $\chi^2_{4M_P}$ and empirical (solid) cumulative and complementary cumulative distribution functions of the interior (blue) and boundary (red) field energy or intensity for the scanned data in Figure 7, after normalization by their respective standard deviations. The Figure also lists the values of the distribution parameters M_U and M_P at this frequency, as estimated from the data by means of the statistical moment method based on the sample mean and sample standard deviation. Both values M_U and M_P are similar – ideally identical [1], [2] – but significantly smaller than 1 because of the absence of ensemble averaging (stirring) for this static cavity. The results suggest that, despite the inhomogeneity of the tangential boundary H-field, the spatial distribution of the boundary energy of the static cavity is close to what can be expected for a randomized (stirred) boundary field, albeit with a lower number of degrees of freedom than for a stirred field.

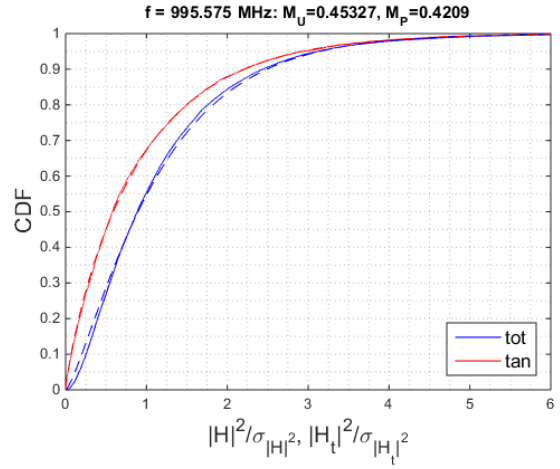

(a)

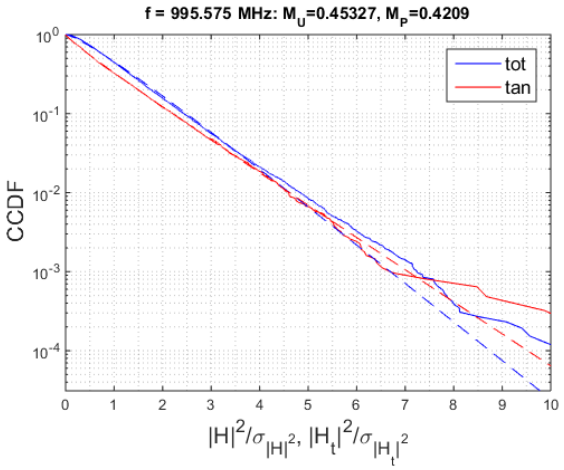

(b)

Figure 8: Theoretical (dashed) $\chi^2_{6M_U}$ and $\chi^2_{4M_P}$ and empirical (solid) distributions for the standardized stored (blue) and dissipated (red) energies or intensities associated with the data of Figure 7: (a) cumulative (CDF) and (b) complementary cumulative (CCDF) distribution functions.

5. Conclusion

In this work, we obtained data from full-wave time-domain simulations inside a highly overmoded reverberant lossy cavity across a narrow (1%) bandwidth. These were used to derive the stored and dissipated energies for estimating *Q* numerically from the magnetic field inside the cavity and on its boundary. It was found that *Q(f)* exhibits rapid spectral fluctuations and that the magnitude of the fluctuations of *Q(f)* rapidly increases with increasing wall conductivity.

The empirical spatial probability distributions of the individual stored and dissipated energies were obtained and compared against respective χ^2 ensemble distributions for ideal statistically homogeneous isotropic circular Gaussian random fields. Despite the regular pseudo-random, but complex nature of the field pattern as demonstrated in Figure 3, it was found that the spatial probability distributions can still be applied, similar to those used for representing ensemble random fields, albeit with different (lower) values for their degrees of freedom. This indicates that, in the simulated frequency band, the spatial pseudo-random process for this static integrable cavity is still well away from the ergodic limit, despite the good agreement with theoretical χ^2 (or, more generally, gamma) distributions.

From the scan data plots in the absence of source or other stirring (ensemble generation), it was found that the tangential boundary magnetic energy in the static cavity exhibits considerable spatial inhomogeneity across the surfaces, even in highly overmoded conditions (λ / $V^{1/3} \approx$ 0.066). This inhomogeneity can be ascribed to the positon and of the monopole antenna with respect to the cavity walls. Source stirring or renormalization of boundary energy with respect to the dissipated power per wall can be used to increase the statistical homogeneity uniformity).

6. References

1. L. R. Arnaut and G. Gradoni, "Probability distribution of the quality factor of a mode-stirred reverberation chamber," *IEEE Trans. Electromagn. Compat.*, **55**, 1, February 2013, pp. 35-44.

2. L. R. Arnaut, M. I. Andries, P. Besnier and J. Sol, "Evaluation method for uncertainty quantification of the quality factor of mode-stirred reverberation chambers," *IEEE Trans. Antennas Propag.*, **62**, 8, August 2014, pp. 4199-4208.